SOAR: Self-supervision Optimized UAV Action Recognition with Efficient Object-Aware Pretraining

Ruiqi Xian[1], Xiyang Wu[1], Tianrui Guan[1], Xijun Wang[1], Boqing Gong[2] and Dinesh Manocha[1]

Abstract— We introduce SOAR, a novel Self-supervised pretraining algorithm for aerial footage captured by Unmanned Aerial Vehicles (UAVs). We incorporate human object knowledge throughout the pretraining process to enhance UAV video pretraining efficiency and downstream action recognition performance. This is in contrast to prior works that primarily incorporate object information during the fine-tuning stage. Specifically, we first propose a novel object-aware masking strategy designed to retain the visibility of certain patches related to objects throughout the pretraining phase. Second, we introduce an object-aware loss function that utilizes object information to adjust the reconstruction loss, preventing bias towards less informative background patches. In practice, SOAR with a vanilla ViT backbone, outperforms best UAV action recognition models, recording a 9.7% and 21.4% boost in top-1 accuracy on the NEC-Drone and UAV-Human datasets, while delivering an inference speed of 18.7ms per video, making it 2× to 5× faster. Additionally, SOAR obtains comparable accuracy to prior self-supervised learning (SSL) methods while requiring 87.5% less pretraining time and 25% less memory usage. Extended tech report, code, and video can be found at https://gamma.umd.edu/researchdirections/aerialvideos/soar.

I. INTRODUCTION

Unmanned Aerial Vehicles (UAVs) equipped with cameras offer distinct advantages for capturing visual data in remote and challenging environments [1]. These systems are used for different applications, such as human detection [2], tracking [3], action recognition [4], [5], and surveillance [6], [7]. UAVs enable the collection of video sequences for analyzing human actions [8], poses [9], identities [10], and attributes [11], which aid decision-making and subsequent processes [12], [13]. However, UAV footage presents unique challenges in terms of perception and action recognition, as compared to ground-based video, including **(a) Small Human Subjects.** Due to the high altitude of UAVs, human figures occupy only a small fraction of the video frames, as shown in Figure. 1. For instance, in the challenging UAV-Human dataset [14], human subjects cover less than 5% of the frame on average, making it difficult for models to capture fine details of human movement and increasing the risk of over-reliance on background features. **(b) Limited Labeled Data.** Obtaining high-quality labeled data for UAV-based perception tasks is particularly challenging. The unique viewing angles, moving cameras, and small human subjects complicate the annotation process [15], [16], [14], [17], making it difficult to generate robust datasets. Even the largest UAV dataset, UAV-Human, contains only 22k
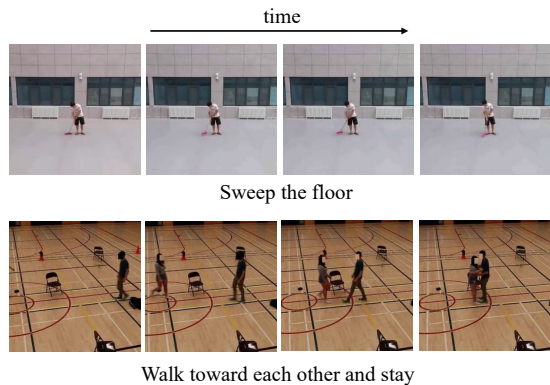

Fig. 1: Typical UAV video Datasets. Example frames from two UAV video datasets: UAV-Human (top) and NEC-Drone (bottom).

videos, which is significantly smaller compared to normal video datasets like Kinetics [18], which has over 300k videos. This data scarcity further hampers the training of deep learning models for UAV-based human action recognition. These challenges necessitate specialized algorithms to understand human behavior accurately from UAV video data, considering its distinct features for effective performance.

Recent research [19], [20], [21], [22] has shown that object-centric approaches in UAV video analysis, particularly those focusing on human subjects and regions of interest (ROIs), can significantly boost recognition performance. However, these methods typically incorporate object knowledge during the fine-tuning stage, often requiring additional steps such as generating bounding boxes or feature alignment, which can increase computational demands and slow down inference. In contrast, we propose leveraging object knowledge during the self-supervised pretraining phase, allowing for fine-tuning on downstream tasks without the need for extra procedures, resulting in a simpler, more efficient inference process.

Main Contributions: In this paper, we introduce SOAR, a novel approach that leverages object knowledge within videos to enhance the the self-supervised pre-training phase through masked autoencoding (MAE) [23], [24]. Our method specifically addresses the challenge posed by UAV videos, where human subjects occupy only a small portion of the visual field. Our main contributions include:

- We propose an innovative object-aware masking strategy that leverages the object information to guide the masking process. It ensures the preservation of patches associated with objects during the pre-training phase so that the model can learn spatiotemporal patterns relevant to the objects more effectively and efficiently.

[1]Authors are with University of Maryland-College Park, MD, USA rxian@umd.edu
[2]Author is with Boston University, MA,USA

- We introduce an object-aware loss function that leverages knowledge about objects to adjust the reconstruction loss. This recalibration prevents the model from developing a bias towards predominant background patches, which provide minimal semantic information about human actions.
- We present SOAR, a novel self-supervised pretraining algorithm that reduces memory usage and accelerates the pre-training process. Additionally, SOAR improves accuracy in downstream UAV action recognition tasks without introducing any inference overhead, offering a faster, end-to-end inference process compared to existing methods that rely on additional data augmentation or detection stages.

In practice, SOAR outperforms existing state-of-the-art supervised methods, recording a 9.7% improvement in top-1 accuracy on the NEC-Drone dataset and a 21.4% increase on UAV-Human with 2x to 5x faster inference speed. When compared with state-of-the-art self-supervised methods, SOAR demonstrates a 2.0% accuracy improvement on NEC Drone and a 4.3% performance boost on UAV-Human. Notably, our method achieves accuracy levels comparable to previous self-supervised learning (SSL) methods, but with an 87.5% reduction in pre-training time and 25% lower memory.

II. RELATED WORK

Action Recognition for UAV Videos. Deep learning has significantly improved action recognition in ground-based videos [25], [26], [27], [28], [29], [30], [31] but faces challenges in UAV videos due to factors like camera movement, varied viewpoints, and small object sizes [32]. Approaches using 2D CNNs, such as ResNet [33] and MobileNet [34], process individual frames and fuse the results [35], [8], [36], while dual-stream CNN models capture both motion and appearance [4], [37]. To tackle temporal complexities, 3D CNNs [38], [14], [8], [39] have been used to analyze spatial-temporal dimensions. Recently, methods like AZTR [19] combine CNNs with attention mechanisms for resource-efficient action recognition. Other techniques, such as Fourier-based attention [21], [40], enhance motion salience. In contrast, our method optimizes pretraining to streamline the process, using raw RGB data without adding complexity during fine-tuning or inference.

Object-based Video Representation. Using object details in video recognition is a growing trend [41], [42], with techniques incorporating RoI features [43] and off-the-shelf detectors in feature banks [44], [45]. Advances in transformers, such as ORViT [46], have led to object-aware representations through cropped object tokens [47] or object-to-pixel transformers [48]. Some models even omit visual inputs entirely [49], [50]. However, these methods primarily focus on general videos, not UAV-specific data with broader fields of view and irrelevant objects. Our approach, instead, leverages human object information in the pretraining phase, addressing the specific challenges of UAV videos.

Masked Visual Modeling. Masking techniques have evolved from early autoencoders [51] to recent Transformer-based models like BEiT [52] and VideoMAE [24], which mask tokens for visual learning. VideoMAE introduced tube masking to increase reconstruction difficulty [24], followed by innovations like MAR [22] to reduce training costs and VideoMAE V2 [53] to scale pretraining efficiency. Some strategies use motion-guided masking for temporal consistency [54]. Our approach, however, is simpler and more memory-efficient, focusing on human-object bounding boxes rather than techniques like optical flow, making it particularly suited to the UAV context with its dynamic camera movements.

III. METHODOLOGY

In this section, we introduce our proposed SOAR method. First, we discuss how UAV video analysis entails a long-tailed learning issue and how its characteristics challenge existing masked autoencoding methods in Section III-A. We then present an overview of our proposed SOAR in Section III-B. Our novel-designed object-aware masking and object-aware loss are further explained in Section III-C and Section III-D, respectively.

A. Problem Formulation

Pretraining UAV videos using masked autoencoders, where self-supervision relies on reconstructing masked patches, faces a unique challenge due to the UAV data's inherent imbalance. Unlike traditional video datasets, UAV data presents a long-tailed distribution in the following sense. The tokens (or video patches) related to human (tail) form a small portion compared to the dominant background (head).

This imbalance creates a long-tailed learning problem. The model, exposed to significantly more head class data, prioritizes learning from background features, neglecting crucial information from the under-represented tail class. This bias hinders the model's ability to perform well on tasks like human action recognition, where the key information lies in the spatiotemporal patterns of human motion that are primarily contained within the tail class data.

To address this challenge, we explore how object knowledge can benefit UAV video pre-training. We focus on two key questions:

- **Balanced Patch Selection.** How to strategically select unmasked patches for a balanced distribution between human-related and background tokens during pretraining?
- **Mitigating Bias.** How to utilize object knowledge to guide the model towards learning from patches related to the human object, reducing bias towards the dominant background?

As UAV videos have a larger field of view, containing many objects that are not related to the actions, our approach focuses solely on human objects.

B. Overall learning Method

Our proposed method, SOAR, processes both video data and object detection information. As illustrated in Figure 2, SOAR masks random video patches and reconstructs the
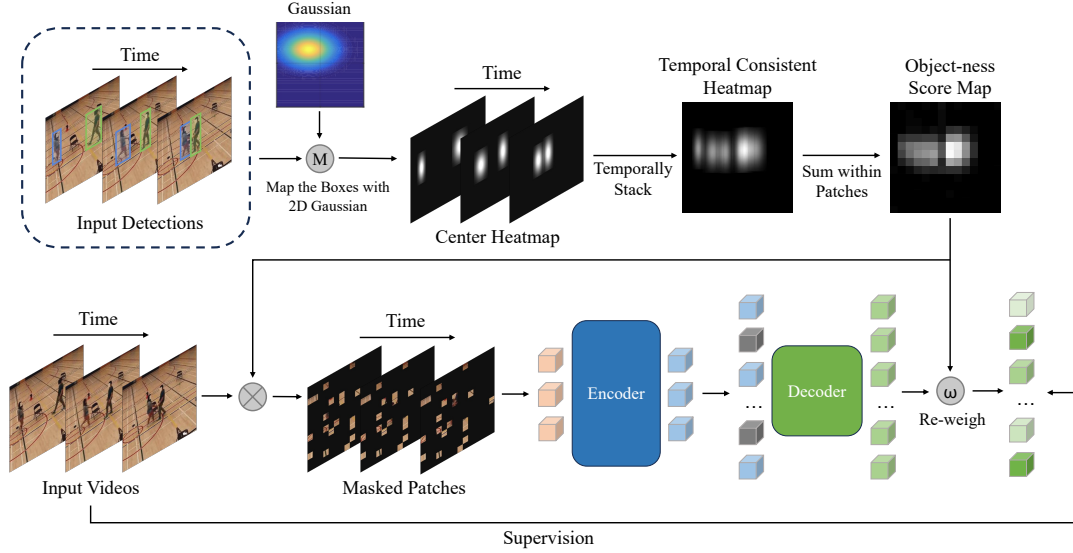
Fig. 2: Overview of SOAR. SOAR uses an asymmetric encoder-decoder architecture to mask random video patches and reconstruct the missing ones, while leveraging object information to optimize the reconstruction. It takes both video frames and object detections as input. It first generates a center heatmap for each frame using 2D Gaussians for each bounding box. These heatmaps are then temporally stacked, and pixel values within patches are summed to create an objectness score map. This map serves a dual purpose: guiding the object-aware masking strategy to ensure balanced patch masking and contributing to the object-aware loss function to reweigh the reconstruction loss.

missing ones using an asymmetric encoder-decoder architecture, while also leveraging object information to optimize the reconstruction process. Note that, The input detections come from widely available off-the-shelf detectors with no finetuning on downstream datasets.

The process begins by splitting an input video $V \in \mathbb{R}^{T \times C \times H \times W}$, where T, C, H, W denote the number of frames, channels, height, and width, into non-overlapping patches $P = \{P_i \| P_i \in \mathbb{R}^{t \times C \times h \times w}\}_{i=1}^N$, with $N = \frac{T}{t} \times \frac{H}{h} \times \frac{W}{w}$ being the total patch count. These patches are converted into a sequence of tokens $K = \{K_i | K_i \in \mathbb{R}^D\}_{i=1}^N$ through patch embedding and positional encoding.

An object-ness score map is generated from the input detections to produce a binary mask M, identifying visible patches for reconstruction through our object-aware masking strategy (detailed in Section. III-C. The encoder Φ_{enc}, a ViT with space-time attention, processes visible tokens K^{vis} to produce latent features $F = \Phi_{enc}(K^{vis}) \in \mathbb{R}^{N_{vis} \times D}$. The latent feature F and the masked tokens K^{inv} are then concatenated into one sequence and decoded by Φ_{dec}, a shallower ViT, to reconstruct the video $\hat{V}$.

The object-ness score map is also used to create our proposed object-aware loss function, described in Section. III-D. Training minimizes the Object-aware loss between the original V and reconstructed $\hat{V}$ over masked areas. The encoder is then applied for fine-tuning in downstream action recognition tasks.

C. Object-Aware Masking

In this section, we introduce our object-aware masking strategy which utilizes the human object information to achieve a balanced patch selection between human-related and background tokens. Besides the input video $V \in \mathbb{R}^{T \times C \times H \times W}$, we include human object detections

$\mathbb{B} = \{\{b_{t,i}\}_{i=1}^{n_t}\}_{t=1}^T$ where $b_{t,i} = (x_{t,i}^c, y_{t,i}^c, x_{t,i}^s, y_{t,i}^s)$ is the bounding box of the $i - th$ human object in frame t with $(x_{t,i}^c, y_{t,i}^c), (x_{t,i}^s, y_{t,i}^s)$ representing the center and size of the bounding box. The bounding box can be oracle boxes from annotation for analytic benchmarks or, in our case, from an off-the-shelf object detector [55]. By incorporating this human object detection information, our method aims to achieve an informed masking strategy. Note that we do not need object detection during inference for efficiency.

We generate a continuous pixel-wise objectness score heatmap. This map reflects the spatial proximity of each pixel to the center of the bounding boxes associated with the detected human objects. Essentially, it transforms objects in the videos into a single, class-agnostic heatmap. Specifically, we first initialize a heatmap for every bounding box $b_{t,i} \in \mathbb{B}$ in the original image resolution but with all pixel values equal to zero. Then, we introduce a 2D Gaussian with the same center and "size" as the bounding box into the heatmap by discretizing it into x^s, y^s points along the x, y-axis. Finally, we sum all the heatmaps for every bounding box and every frame and normalize their values along the temporal dimension to obtain the overall pixel-wise objectness score heatmap $H \in \mathbb{R}^{H \times W}$:

$$H = \frac{1}{T} \sum_t^T \sum_i^{n_t} \exp\left(-\frac{(x - x_{t,i}^c)^2 + (y - y_{t,i}^c)^2}{2\sigma^2}\right)$$

where σ is the standard deviation of the Gaussian that controls the peak and radius of the Gaussian.

Next, we derive patch-level objectness from the pixel-level objectness heatmap H by segmenting it into patches matching our video patch size and summing up pixel scores within each patch. The compiled patch-level objectness heatmap, $\mathbb{H} \in \mathbb{R}^{\frac{W}{w} \times \frac{H}{h}}$, essentially reflects the total duration or
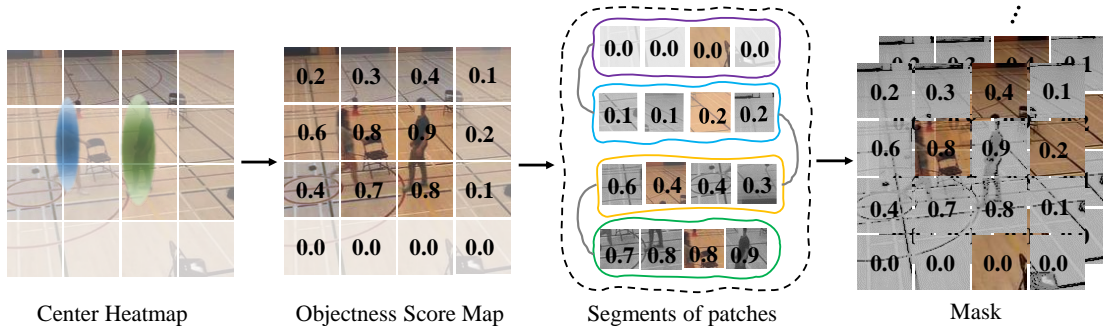
Fig. 3: Our Object-Aware Masking Strategy. We first render the patch-level object core map from the center heatmap, then sort all the patches based on their corresponding objectness scores. The sorted patches are divided into segments of equal length. Within each segment, one patch is randomly chosen to remain unmasked, while the remaining patches are masked. Finally, the generated mask is replicated across the temporal dimension to avoid information leakage.

prevalence of a human object appearing within that specific patch throughout the video.

As mentioned in Section. III-A, ensuring a balanced distribution of unmasked patches is crucial. As illustrated in Figure 3, we begin by sorting all the patches based on their corresponding objectness scores and partition the sorted patches into $(1-\rho)(\frac{W}{w} \times \frac{H}{h})$ segments of equal length. Within each segment, we randomly select one patch to be unmasked, while all remaining patches in that segment are masked. The resulting spatial mask map is replicated $\frac{H}{h}$ times along the temporal dimension to account for video sequences. Finally, the mask is flattened into a one-dimensional binary mask $M \in \mathbb{R}^N$.

This object-aware masking strategy lowers the probability of masking human object-related patches and guarantees a minimum number of human-related patches remain unmasked. This adaptive approach helps maintain the visibility of crucial human movement information during the pretraining so that the encoder can learn more spatiotemporal patterns related to the human object.

D. Object-Aware Loss

In this section, we introduce our object-aware loss function, designed to leverage object-centric knowledge and reduce the model's bias towards the dominant background. Like previous methods [24], [53], we start with the Mean Square Error (MSE) loss, assessing the difference between the original and reconstructed videos at masked locations. Our innovation adjusts this loss by including patch-level objectness scores for a more equitable training approach.

We overlook unmasked tokens, irrelevant for reconstruction, and focus on the objectness scores S^{inv} for masked patches. To ensure that background patches contribute minimally to the loss as they still contain valuable environmental information, we add the mean μ of all objectness scores to each score. This prevents masked patches with zero objectness scores (pure background) from being entirely ignored during training. Then, we normalize the objectness scores by their sum, making their sum equal to 1. These normalized scores then act as weights to re-balance the MSE loss:

$$\mathcal{L}_{new} = \sum_{i \in K^{inv}} \frac{S_i^{inv} + \mu}{\sum_i \left(S_i^{inv} + \mu \right)} \|V_i - \hat{V}_i\|^2$$

where S_i^{inv} is the object-ness score corresponding to the $i-th$ invisible patch. By integrating the objectness scores, this refined loss function steers the model's focus towards regions containing objects, particularly human objects in UAV videos. This encourages a more balanced learning dynamic by mitigating the bias towards the dominant background and directing the model to prioritize learning from crucial object-related information.

IV. EXPERIMENTS

A. Datasets

UAV-Human [14], the most comprehensive UAV dataset for human behavior analysis, contains 22,476 HD videos from diverse indoor and outdoor environments with 155 annotated actions. It presents challenges like dynamic backgrounds and varying lighting conditions.

NEC-Drone [39], consists of 5,250 videos with 16 actions captured in a basketball court using a low-altitude UAV with light reflection noise despite consistent lighting.

B. Implementation Details

The results presented in this section are based on either a 12-layer ViT-Base or a 24-layer ViT-Large model for the encoder, with an 8-layer narrow ViT as the decoder. Both the encoder and decoder are initialized with Kinetics400 weights, pretrained for 800 epochs. During pretraining, the model is further trained on UAV datasets for 400 epochs, using 16 frames at a resolution of 224×224. Following pretraining, the encoder is fine-tuned for 100 epochs on downstream tasks. Dense sampling is applied during fine-tuning, and results are reported using a uniform inference protocol of 5 clips × 3 crops.

C. Main Results and Analysis

Comparison with State-of-the-Art Supervised Methods. We compared SOAR with current state-of-the-art methods on the NEC-Drone and UAV-Human datasets, as summarized in Table I. SOAR sets a new benchmark in UAV

Method	Backbone	Extra data	Input Size	Frames	Views	GFLOPs	Params.	NEC-Drone Acc.@1 ↑	UAV-Human Acc.@1 ↑
supervised									
Slowfast [56]	ResNet50	K400	224 × 224	8	5 × 3	99	50M	77.1	36.3
FAR [21]	X3D-M	K400	540 × 960	8	10 × 3	65	4M	71.4	38.6
DiffFAR [40]	X3D-M	K400	540 × 960	8	10 × 3	130	4M	80.7	41.9
AZTR [19]	X3D-M	K400	224 × 224	16	10 × 3	7	4M	-	47.4
MITFAS[20]	X3D-M	K400	224 × 224	16	10 × 3	7	4M	78.6	50.8
PMI Sampler [57]	X3D-M	K400	224 × 224	16	10 × 3	7	4M	62.5	55.0
MViT v1 [58]	MViT-B	K400	224 × 224	16	5 × 1	71	37M	34.6	24.3
ViViT FE [59]	ViT-B	IN-21K	224 × 224	16	1 × 1	284	116M	38.4	34.1
TimesFormer [60]	ViT-B	K400	224 × 224	8	1 × 3	196	131M	40.5	38.4
MotionFormer [61]	ViT-B	IN21K + K400	224 × 224	8	10 × 3	370	109M	73.6	50.4
self-supervised									
ST-MAE [23]	ViT-B	K400	224 × 224	16	5 × 3	180G	87M	-	45.1
VideoMAE [24]	ViT-B	K400	224 × 224	16	5 × 3	180G	87M	82.5	62.1
VideoMAE [24]	ViT-L	K400	224 × 224	16	5 × 3	597G	305M	88.4	71.5
VideoMAE v2 [53]	ViT-G	K400	224 × 224	16	5 × 3	5.1T	632M	82.2	61.1
MVD [62]	ViT-B	IN21K + K400	224 × 224	16	5 × 3	180G	87M	77.6	60.5
SOAR(Ours)	ViT-B	K400	224 × 224	16	5 × 3	180	87M	**84.6**	**66.4**
SOAR(Ours)	ViT-L	K400	224 × 224	16	5 × 3	597G	305M	**90.4**	**76.4**

TABLE I: **Comparison with Previous State-Of-The-Arts Methods on NEC-Drone and UAV-Human.** Our method achieves the best top-1 accuracy on both datasets after finetuning.

video analysis, significantly outperforming previous supervised methods on both datasets. With the ViT-B backbone, SOAR achieved top-1 accuracy improvements of 3.9% on NEC-Drone and 11.4% on UAV-Human. The performance gains were even more substantial with the ViT-L backbone, delivering a 9.7% boost on NEC-Drone and an impressive 21.4% increase on UAV-Human.

SOAR demonstrates the power of self-supervised video pretraining, where models learn from unlabeled videos before fine-tuning on labeled tasks. This approach reduces dependency on large, annotated datasets and allows the model to autonomously discover meaningful visual features, resulting in a deeper understanding of video semantics and improved performance on downstream tasks such as action recognition.

Comparison with State-of-the-Art Self-Supervised Methods. We compared SOAR with other self-supervised methods on the NEC-Drone and UAV-Human datasets (see Table I). With a ViT-B backbone, SOAR significantly outperforms previous video mask autoencoders, achieving 2.1% and 4.3% higher top-1 accuracy on the NEC-Drone and UAV-Human datasets, respectively. When scaled up to a ViT-L backbone, SOAR continues to excel, showing 2.0% and 5.2% accuracy improvements over previous SOTAs on NEC-Drone and UAV-Human, demonstrating consistent scalability. Need to note that, VideoMAE v2 with the considerably larger ViT-G backbone shows limited performance gains. This could be attributed to its dual masking strategy, which significantly increases the likelihood of overlooking human-related patches during reconstruction.

These results highlight the importance of object-aware pretraining in UAV video analysis. Leveraging human object knowledge during pretraining significantly enhances performance, revealing the limitations of approaches that neglect object focus.

Inference Time. We evaluated the inference speed of our SOAR model against two state-of-the-art methods, AZTR [19] and MITFAS [20], using an RTX A5000 GPU. As shown in Table II, SOAR achieves significantly faster

Method	Data Aug.	Backbone	NEC Drone Acc.@1 ↑	UAV-Human Acc.@1 ↑	Inference time /video (ms)
AZTR [19]	✓	X3D-M	-	47.4	37.1
MITFAS [20]	✓	X3D-M	78.6	50.8	92.4
SOAR(Ours)	✗	ViT-B	84.6	66.4	18.7

TABLE II: **Inference Time Comparison.** While inferencing on an RTX A5000 GPU, our method is 2× faster than AZTR and 5× faster than MITFAS.

inference times, processing videos in 18.7 milliseconds per video—2 times faster than AZTR and 5 times faster than MITFAS—while maintaining superior accuracy.

SOAR's efficiency in the inference stage stems from its strategic use of object information during pre-training. Unlike other methods that require additional computational steps during inference, such as online object detection and data augmentation (AZTR) or feature alignment (MITFAS), SOAR only uses bounding boxes in pre-training. This allows it to directly process unmodified video frames during inference, resulting in substantially reduced processing time and making SOAR ideal for real-time applications.

Mask Ratio. We investigate the impact of different mask ratios on UAV video pretraining, with results shown in Figure 4. In contrast to previous studies [53], [24], we found that using a high mask ratio (90%–95%) does not necessarily improve fine-tuning performance for downstream UAV action recognition tasks. This is due to the smaller size of human subjects in UAV footage, limiting the model's ability to learn meaningful human-centric semantics and motion.

Our experiments show that a mask ratio of around 70% provides the best pretraining performance for UAV videos. This ratio offers a balance between challenging the model with partial views and ensuring sufficient visibility of human-related information to effectively capture human dynamics. These findings highlight the need for mask ratios tailored to the unique characteristics of UAV video analysis, rather than relying on the general approach commonly applied in masked autoencoding.

Memory Efficiency. High mask ratios in UAV video pretraining reduce memory usage due to fewer unmasked
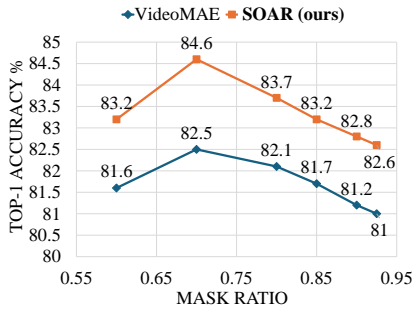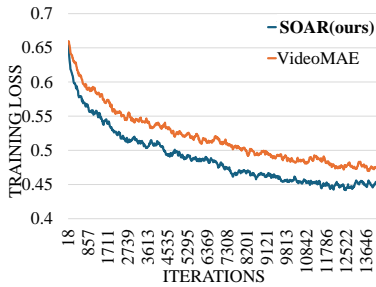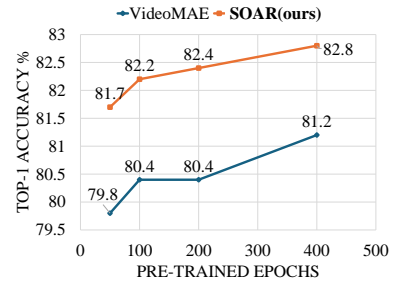
Fig. 4: Top-1 Accuracy under Different Mask Ratios. Contrary to findings from previous studies, a mask ratio of around 70% yields the best accuracy for UAV data.

(a) Training Loss

(b) Accuracy

Fig. 5: Time Efficiency Comparison. SOAR converges much faster during pretraining and shows comparable results with pretraining 87.5% fewer epochs (81.7% accuracy when pretraining 50 epochs vs. 81.2% with 400 epochs).

	NEC-Drone Acc.@1 ↑	UAVHuman Acc.@1 ↑
Vanilla	81.2	62.1
+ OAM	81.7	64.0
+ OAL	82.8	66.4

(a) Design Validation. Both our modules contribute to the performance improvement.

Masking	NEC-Drone	
	Acc.@1 ↑	Acc.@5 ↑
random	80.2	98.6
tube	81.2	98.6
block	80.7	98.6
ours	**82.8**	**99.1**

(b) Masking Strategy. Our method outperforms random, tube and block masking strategy.

Detector	Backbone	CrowdHuman mAP ↑	UAVHuman Acc.@1 ↑
None (Vanilla VideoMAE)	-	-	62.1
Cascade Mask R-CNN	MobileNet	65.7	63.9
Faster R-CNN	HRNet	72.3	65.9
Cascade Mask R-CNN	**HRNet**	**84.1**	**66.4**

(c) Results using different detectors. Our method consistently outperforms previous approaches, even when using lower-quality detections.

TABLE III: Ablation Studies.

tokens needing processing. As Figure 4 demonstrates, SOAR is particularly adept at exploiting this benefit. SOAR achieves comparable accuracy to previous SOTA, even with a substantially higher mask ratio. For instance, SOAR reaches 82.6% accuracy with only 7.5% of tokens unmasked (92.5% mask ratio), while VideoMAE requires 30% unmasked tokens (70% mask ratio) for a similar result. Thus, SOAR is highly memory-efficient, requiring only 25% of the memory compared to VideoMAE, attributed to its strategic focus on critical human-related tokens at higher mask ratios.

Time Efficiency. Our investigation highlights SOAR's superior pre-training time efficiency compared to previous methods, as shown in Figure 5. SOAR demonstrates faster convergence and requires significantly fewer training epochs to achieve comparable results. For instance, on the NEC-Drone dataset, SOAR reaches 81.7% top-1 accuracy within just 50 epochs, while VideoMAE requires 87.5% more epochs (400) to attain a similar 81.2% accuracy. This efficiency is driven by SOAR's object-aware masking and loss function, which prioritize human-centric information during training. By focusing on key human elements, SOAR accelerates the learning process and enhances pre-training effectiveness for UAV action recognition tasks.

D. Ablation Studies

Effectiveness of Both Designs. In a step-wise evaluation detailed in Table IIIa, we analyzed the impact of the object-aware masking strategy (OAM) and the object-aware loss

function (OAL) by pre-training two models: one using only OAM and another using both OAM and OAL. The results demonstrate the effectiveness of each component, with OAM alone boosting accuracy by 0.5% on NEC-Drone and 1.9% on UAV-Human. The addition of OAL further improved accuracy, yielding an additional 1.1% on NEC-Drone and 2.4% on UAV-Human. These findings highlight the combined contributions of OAM and OAL in enhancing performance for UAV action recognition tasks.

Comparison with Other Masking Strategies. We compared our object-aware masking strategy against conventional methods such as random, tube, and block masking, evaluating both reconstruction quality and action recognition performance. As shown in Table IIIb, our approach consistently outperforms these traditional methods.

Impact of Bounding Box Quality. Table IIIc presents additional results using different off-the-shelf detectors (trained on CrowdHuman and zero-shot on UAVHuman). While the quality of the bounding boxes influences the final accuracy, our method consistently outperforms previous approaches that do not incorporate object cues.

More results and analysis are in the tech report on the project page.

V. CONCLUSION, LIMITATIONS, AND FUTURE WORK

In this paper, we introduced SOAR, a novel approach that leverages object knowledge to optimize the video pre-training process, leading to improved performance in downstream action recognition tasks for UAV videos. SOAR incorporates two key innovations: an object-aware masking strategy and an object-aware loss function. Empirical results show that SOAR effectively sets new benchmarks on the NEC-Drone and UAV-Human datasets, demonstrating its simplicity and effectiveness for UAV video analysis.

Despite its strong performance, our method has certain limitations. Currently, SOAR is designed specifically for transformer architectures, as the masking and reconstruction processes operate at the token level. Expanding SOAR to more edge-device-friendly architectures, such as CNNs, is a promising direction for future work. Additionally, further evaluation and tighter integration with UAV hardware will be necessary to assess SOAR's practicality and efficiency in real-world UAV systems.

REFERENCES

[1] H. Zhao, H. Wang, W. Wu, and J. Wei, "Deployment algorithms for uav airborne networks toward on-demand coverage," *IEEE Journal on Selected Areas in Communications*, vol. 36, no. 9, pp. 2015–2031, 2018.

[2] Y. Gong, X. Yu, Y. Ding, X. Peng, J. Zhao, and Z. Han, "Effective fusion factor in fpn for tiny object detection," 2020.

[3] Y. Wang, L. Ding, and R. Laganiere, "Real-time uav tracking based on psr stability," in *Proceedings of the IEEE/CVF International Conference on Computer Vision Workshops*, 2019, pp. 0–0.

[4] A. G. Perera, Y. W. Law, and J. Chahl, "Drone-action: An outdoor recorded drone video dataset for action recognition," *Drones*, vol. 3, no. 4, p. 82, 2019.

[5] ——, "Uav-gesture: A dataset for uav control and gesture recognition," 2019.

[6] M. Schwager, B. J. Julian, M. Angermann, and D. Rus, "Eyes in the sky: Decentralized control for the deployment of robotic camera networks," *Proceedings of the IEEE*, vol. 99, no. 9, pp. 1541–1561, 2011.

[7] P. Zhu, L. Wen, D. Du, X. Bian, H. Fan, Q. Hu, and H. Ling, "Detection and tracking meet drones challenge," *IEEE Transactions on Pattern Analysis and Machine Intelligence*, vol. 44, no. 11, pp. 7380–7399, 2021.

[8] H. Mliki, F. Bouhlel, and M. Hammami, "Human activity recognition from uav-captured video sequences," *Pattern Recognition (PR)*, vol. 100, p. 107140, 2020.

[9] J. P. T. Sien, K. H. Lim, and P.-I. Au, "Deep learning in gait recognition for drone surveillance system," *IOP Conference Series: Materials Science and Engineering*, vol. 495, no. 1, p. 012031, apr 2019. [Online]. Available: https://dx.doi.org/10.1088/1757-899X/495/1/012031

[10] A. Deeb, K. Roy, and K. D. Edoh, "Drone-based face recognition using deep learning," in *Advanced Machine Learning Technologies and Applications: Proceedings of AMLTA 2020*. Springer, 2021, pp. 197–206.

[11] J. Liu, B. Kuipers, and S. Savarese, "Recognizing human actions by attributes," in *CVPR 2011*. IEEE, 2011, pp. 3337–3344.

[12] J. Hoey and J. J. Little, "Value-directed human behavior analysis from video using partially observable markov decision processes," *IEEE transactions on pattern analysis and machine intelligence*, vol. 29, no. 7, pp. 1118–1132, 2007.

[13] J. Supancic III and D. Ramanan, "Tracking as online decision-making: Learning a policy from streaming videos with reinforcement learning," in *Proceedings of the IEEE international conference on computer vision*, 2017, pp. 322–331.

[14] T. Li, J. Liu, W. Zhang, Y. Ni, W. Wang, and Z. Li, "Uav-human: A large benchmark for human behavior understanding with unmanned aerial vehicles," in *IEEE/CVF Conference on Computer Vision and Pattern Recognition (CVPR)*, 2021, pp. 16 266–16 275.

[15] M. Barekatain, M. Martí, H.-F. Shih, S. Murray, K. Nakayama, Y. Matsuo, and H. Prendinger, "Okutama-action: An aerial view video dataset for concurrent human action detection," in *Proceedings of the IEEE conference on computer vision and pattern recognition workshops*, 2017, pp. 28–35.

[16] P. Burdziakowski, "A novel method for the deblurring of photogrammetric images using conditional generative adversarial networks," *Remote Sensing*, vol. 12, no. 16, p. 2586, 2020.

[17] A. Walha, A. Wali, and A. M. Alimi, "Video stabilization with moving object detecting and tracking for aerial video surveillance," *Multimedia Tools and Applications*, vol. 74, pp. 6745–6767, 2015.

[18] W. Kay, J. Carreira, K. Simonyan, B. Zhang, C. Hillier, S. Vijayanarasimhan, F. Viola, T. Green, T. Back, P. Natsev *et al.*, "The kinetics human action video dataset," *arXiv preprint arXiv:1705.06950*, 2017.

[19] X. Wang, R. Xian, T. Guan, C. M. de Melo, S. M. Nogar, A. Bera, and D. Manocha, "Aztr: Aerial video action recognition with auto zoom and temporal reasoning," *2023 IEEE International Conference on Robotics and Automation (ICRA)*, pp. 1312–1318, 2023. [Online]. Available: https://api.semanticscholar.org/CorpusID:257353660

[20] R. Xian, X. Wang, and D. Manocha, "Mitfas: Mutual information based temporal feature alignment and sampling for aerial video action recognition," in *Proceedings of the IEEE/CVF Winter Conference on Applications of Computer Vision*, 2024, pp. 6625–6634.

[21] D. Kothandaraman, T. Guan, X. Wang, S. Hu, M. Lin, and D. Manocha, "Far: Fourier aerial video recognition," in *Computer Vision – ECCV 2022*, S. Avidan, G. Brostow, M. Cissé, G. M.

Farinella, and T. Hassner, Eds. Cham: Springer Nature Switzerland, 2022, pp. 657–676.

[22] Z. Qing, S. Zhang, Z. Huang, X. Wang, Y. Wang, Y. Lv, C. Gao, and N. Sang, "Mar: Masked autoencoders for efficient action recognition," *IEEE Transactions on Multimedia*, 2023.

[23] C. Feichtenhofer, Y. Li, K. He *et al.*, "Masked autoencoders as spatiotemporal learners," *Advances in neural information processing systems*, vol. 35, pp. 35 946–35 958, 2022.

[24] Z. Tong, Y. Song, J. Wang, and L. Wang, "Videomae: Masked autoencoders are data-efficient learners for self-supervised video pretraining," *Advances in neural information processing systems*, vol. 35, pp. 10 078–10 093, 2022.

[25] F. Rezazadegan, S. Shirazi, B. Upcroft, and M. Milford, "Action recognition: From static datasets to moving robots," in *2017 IEEE International Conference on Robotics and Automation (ICRA)*. IEEE, 2017, pp. 3185–3191.

[26] N. Soans, E. Asali, Y. Hong, and P. Doshi, "Sa-net: Robust state-action recognition for learning from observations," in *2020 IEEE International Conference on Robotics and Automation (ICRA)*. IEEE, 2020, pp. 2153–2159.

[27] B. van Amsterdam, M. J. Clarkson, and D. Stoyanov, "Multi-task recurrent neural network for surgical gesture recognition and progress prediction," in *2020 IEEE International Conference on Robotics and Automation (ICRA)*. IEEE, 2020, pp. 1380–1386.

[28] J. Massardi, M. Gravel, and É. Beaudry, "Parc: A plan and activity recognition component for assistive robots," in *2020 IEEE International Conference on Robotics and Automation (ICRA)*. IEEE, 2020, pp. 3025–3031.

[29] L. Yao, S. Liu, C. Li, S. Zou, S. Chen, and D. Guan, "Pa-awcnn: Two-stream parallel attention adaptive weight network for rgb-d action recognition," in *2022 International Conference on Robotics and Automation (ICRA)*. IEEE, 2022, pp. 8741–8747.

[30] Z. Shao, Y. Li, Y. Guo, J. Yang, and Z. Wang, "A hierarchical model for action recognition based on body parts," in *2018 IEEE international conference on robotics and automation (ICRA)*. IEEE, 2018, pp. 1978–1985.

[31] C. Lea, R. Vidal, and G. D. Hager, "Learning convolutional action primitives for fine-grained action recognition," in *2016 IEEE international conference on robotics and automation (ICRA)*. IEEE, 2016, pp. 1642–1649.

[32] K. Nguyen, C. Fookes, S. Sridharan, Y. Tian, X. Liu, F. Liu, and A. Ross, "The state of aerial surveillance: A survey," *arXiv preprint arXiv:2201.03080*, 2022.

[33] K. He, X. Zhang, S. Ren, and J. Sun, "Deep residual learning for image recognition," in *Proceedings of the IEEE Conference on Computer Vision and Pattern Recognition (CVPR)*, June 2016.

[34] A. G. Howard, M. Zhu, B. Chen, D. Kalenichenko, W. Wang, T. Weyand, M. Andreetto, and H. Adam, "Mobilenets: Efficient convolutional neural networks for mobile vision applications," 2017.

[35] L. Mou, L. Hua, P. Jin, and X. X. Zhu, "Event and activity recognition in aerial videos using deep neural networks and a new dataset," in *IGARSS 2020-2020 IEEE International Geoscience and Remote Sensing Symposium (IGARSS)*. IEEE, 2020, pp. 952–955.

[36] B. Mishra, D. Garg, P. Narang, and V. Mishra, "Drone-surveillance for search and rescue in natural disaster," *Computer Communications*, vol. 156, pp. 1–10, 2020.

[37] A. G. Perera, Y. W. Law, T. T. Ogunwa, and J. Chahl, "A multiviewpoint outdoor dataset for human action recognition," *IEEE Transactions on Human-Machine Systems*, vol. 50, no. 5, pp. 405–413, 2020.

[38] W. Sultani and M. Shah, "Human action recognition in drone videos using a few aerial training examples," *Computer Vision and Image Understanding*, vol. 206, p. 103186, 2021.

[39] J. Choi, G. Sharma, M. Chandraker, and J.-B. Huang, "Unsupervised and semi-supervised domain adaptation for action recognition from drones," in *IEEE/CVF Winter Conference on Applications of Computer Vision (WACV)*, 2020, pp. 1717–1726.

[40] D. Kothandaraman, M. Lin, and D. Manocha, "Diffar: Differentiable frequency-based disentanglement for aerial video action recognition," in *2023 IEEE International Conference on Robotics and Automation (ICRA)*, 2023, pp. 8254–8261.

[41] G. F. Elsayed, A. Mahendran, S. van Steenkiste, K. Greff, M. C. Mozer, and T. Kipf, "SAVi++: Towards end-to-end object-centric learning from real-world videos," in *Advances in Neural Information Processing Systems*, A. H. Oh, A. Agarwal,

D. Belgrave, and K. Cho, Eds., 2022. [Online]. Available: https://openreview.net/forum?id=fT9W53lLxNS

[42] F. Locatello, D. Weissenborn, T. Unterthiner, A. Mahendran, G. Heigold, J. Uszkoreit, A. Dosovitskiy, and T. Kipf, "Object-centric learning with slot attention," in *Advances in Neural Information Processing Systems*, H. Larochelle, M. Ranzato, R. Hadsell, M. Balcan, and H. Lin, Eds., vol. 33. Curran Associates, Inc., 2020, pp. 11 525–11 538. [Online]. Available: https://proceedings.neurips.cc/paper_files/paper/2020/file/8511df98c02ab60aea1b2356c013bc0f-Paper.pdf

[43] X. Wang and A. Gupta, "Videos as space-time region graphs," in *Proceedings of the European Conference on Computer Vision (ECCV)*, September 2018.

[44] C.-Y. Wu, C. Feichtenhofer, H. Fan, K. He, P. Krähenbühl, and R. Girshick, "Long-Term Feature Banks for Detailed Video Understanding," in *CVPR*, 2019.

[45] C.-Y. Wu and P. Krähenbühl, "Towards long-form video understanding," in *2021 IEEE/CVF Conference on Computer Vision and Pattern Recognition (CVPR)*, 2021, pp. 1884–1894.

[46] R. Herzig, E. Ben-Avraham, K. Mangalam, A. Bar, G. Chechik, A. Rohrbach, T. Darrell, and A. Globerson, "Object-region video transformers," 2021.

[47] K. He, G. Gkioxari, P. Dollár, and R. Girshick, "Mask r-cnn," in *2017 IEEE International Conference on Computer Vision (ICCV)*, 2017, pp. 2980–2988.

[48] C. Zhang, A. Gupta, and A. Zisserman, "Is an object-centric video representation beneficial for transfer?" in *Proceedings of the Asian Conference on Computer Vision*, 2022, pp. 1976–1994.

[49] J. Materzynska, T. Xiao, R. Herzig, H. Xu, X. Wang, and T. Darrell, "Something-else: Compositional action recognition with spatial-temporal interaction networks," in *Proceedings of the IEEE/CVF Conference on Computer Vision and Pattern Recognition*, 2020, pp. 1049–1059.

[50] G. Radevski, M.-F. Moens, and T. Tuytelaars, "Revisiting spatio-temporal layouts for compositional action recognition," *arXiv preprint arXiv:2111.01936*, 2021.

[51] P. Vincent, H. Larochelle, Y. Bengio, and P.-A. Manzagol, "Extracting and composing robust features with denoising autoencoders," in *Proceedings of the 25th international conference on Machine learning*, 2008, pp. 1096–1103.

[52] H. Bao, L. Dong, S. Piao, and F. Wei, "Beit: Bert pre-training of image transformers," *arXiv preprint arXiv:2106.08254*, 2021.

[53] L. Wang, B. Huang, Z. Zhao, Z. Tong, Y. He, Y. Wang, Y. Wang, and Y. Qiao, "Videomae v2: Scaling video masked autoencoders with dual masking," in *Proceedings of the IEEE/CVF Conference on Computer Vision and Pattern Recognition*, 2023, pp. 14 549–14 560.

[54] B. Huang, Z. Zhao, G. Zhang, Y. Qiao, and L. Wang, "Mgmae: Motion guided masking for video masked autoencoding," in *Proceedings of the IEEE/CVF International Conference on Computer Vision*, 2023, pp. 13 493–13 504.

[55] I. Hasan, S. Liao, J. Li, S. U. Akram, and L. Shao, "Generalizable pedestrian detection: The elephant in the room," in *Proceedings of the IEEE/CVF Conference on Computer Vision and Pattern Recognition (CVPR)*, June 2021, pp. 11 328–11 337.

[56] C. Feichtenhofer, H. Fan, J. Malik, and K. He, "Slowfast networks for video recognition," in *Proceedings of the IEEE/CVF International Conference on Computer Vision (ICCV)*, October 2019.

[57] R. Xian, X. Wang, D. Kothandaraman, and D. Manocha, "Pmi sampler: Patch similarity guided frame selection for aerial action recognition," in *Proceedings of the IEEE/CVF Winter Conference on Applications of Computer Vision (WACV)*, January 2024, pp. 6982–6991.

[58] H. Fan, B. Xiong, K. Mangalam, Y. Li, Z. Yan, J. Malik, and C. Feichtenhofer, "Multiscale vision transformers," in *Proceedings of the IEEE/CVF International Conference on Computer Vision (ICCV)*, October 2021, pp. 6824–6835.

[59] A. Arnab, M. Dehghani, G. Heigold, C. Sun, M. Lucic, and C. Schmid, "Vivit: A video vision transformer," *2021 IEEE/CVF International Conference on Computer Vision (ICCV)*, pp. 6816–6826, 2021. [Online]. Available: https://api.semanticscholar.org/CorpusID:232417054

[60] G. Bertasius, H. Wang, and L. Torresani, "Is space-time attention all you need for video understanding?" in *Proceedings of the International Conference on Machine Learning (ICML)*, July 2021.

[61] M. Patrick, D. Campbell, Y. Asano, I. Misra, F. Metze, C. Feichtenhofer, A. Vedaldi, and J. F. Henriques, "Keeping your eye on the ball: Trajectory attention in video transformers," in *Advances in Neural Information Processing Systems*, A. Beygelzimer, Y. Dauphin, P. Liang, and J. W. Vaughan, Eds., 2021. [Online]. Available: https://openreview.net/forum?id=mfQxdSMWOF

[62] R. Wang, D. Chen, Z. Wu, Y. Chen, X. Dai, M. Liu, L. Yuan, and Y.-G. Jiang, "Masked video distillation: Rethinking masked feature modeling for self-supervised video representation learning," in *CVPR*, 2023.